Supporting Information for

High mobility graphene ion-sensitive field-effect transistors by noncovalent functionalization

W. Fu,[*,†] C. Nef,[†] A. Tarasov,[†] M. Wipf,[†] R. Stoop,[†] O. Knopfmacher,[†,‡] M. Weiss,[†] M. Calame,[†] and C. Schönenberger[*,†]

Department of Physics, University of Basel, Klingelbergstrasse 82, CH-4056 Basel, Switzerland

E-mail: Wangyang.Fu@unibas.ch; Christian.Schoenenberger@unibas.ch

[*]To whom correspondence should be addressed
[†]University of Basel
[‡]Present address: Department of Chemical Engineering, Stanford University, Stanford, California, United States

pH response of as-fabricated and phenol-activated graphene FETs

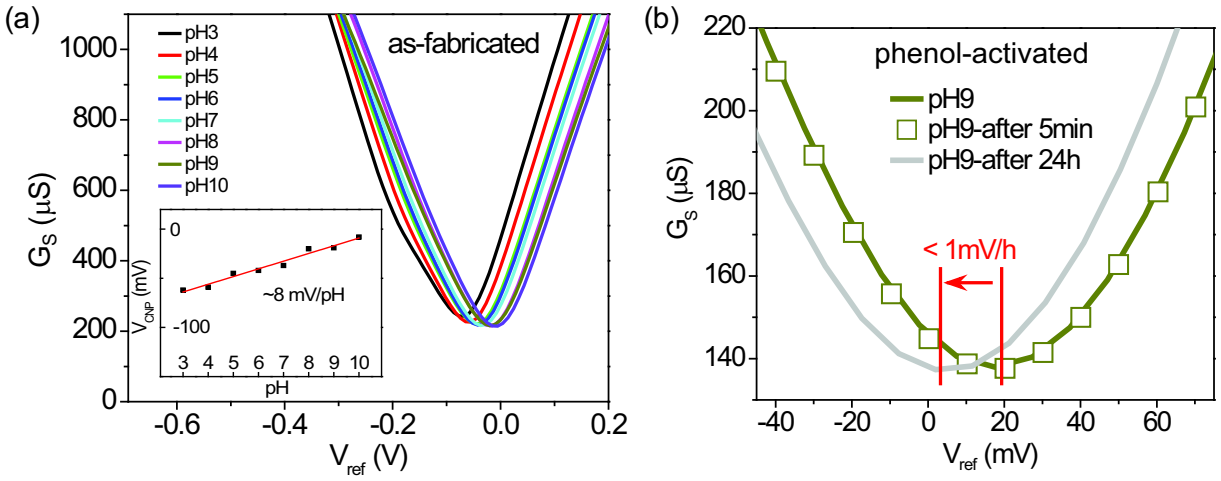

Figure S1: Electrical sheet conductance G_S as a function of the reference potential V_{ref}. (a) Measured in different pH buffer solutions for an as-fabricated graphene FET (the phenol-activated GISFET before functionalization). Inset: The dependence of V_{CNP} versus pH. A weak pH response of 8 mV/pH is observed. (b) Time dependent measurement in pH 9 buffer solutions for the phenol-activated GISFET. Excellent reproducibility (the two continuously measured transfer curves, in dark green, overlap) and stability (the drift of V_{CNP} over 24 h is smaller than 1 mV/h, in comparison to 1 – 2 mV/h of silicon ISFETs. Matsuo et al., *Sensors and Actuators* 1, 77, **1981**), have been demonstrated.

pH response of hybrid phenol-fluorobenzene GISFETs

As a control, we have investigated the pH response of GISFETs with reduced density of adsorbed phenol molecules. This was achieved by a hybrid phenol-fluorobenzene functionalization. The hybrid I sample was realized by immersing a graphene FET device in pure fluorobenzene (30 s) before phenol functionalization (as described in the manuscript). The adsorption of fluorobenzene would lead to a reduction in phenol adsorption afterwards. As shown in Fig. S2c, the pH response of this hybrid I GISFET (blue stars) is significantly reduced comparing with the phenol-activated GISFET (red circles, also shown in Fig. 2b in the manuscript). In case of the hybrid II sample, we applied diluted fluorobenzene (1 M fluorobenzene diluted in ethanol) and a further rinsing in pure ethanol for 5 min before phenol functionalization. We expected that these treatments would reduce the adsorption of fluorobenzene, thus increasing the adsorption of phenol afterwards. As a resut, the pH response of this hybrid II GISFET was enhanced (green triangles, Fig. S2c). But the pH response was still inferior to that of the phenol-activated GISFET (red circles).

By using the single-reaction model, we can fit the pH responses of all the GISFETs. As shown in Figure S2c, the non-linear fitting curves fully agrees with all the data points. An equilibrium constant K_a of phenol can be deduced as $10^{-8.6}$ M for all of the non-linear curves. The fitting to the data also yield $N_s = 5.5 \times 10^{14}\,\mathrm{cm}^{-2}$, $1.2 \times 10^{14}\,\mathrm{cm}^{-2}$, and $3.4 \times 10^{12}\,\mathrm{cm}^{-2}$ for the phenol-activated, hybrid II, and hybrid I GISFETs, respectively. The perfect agreements in between experimental results and the model, suggest ambiguously that the proton sensitivity of the GISFETs is originated from the adsorbed phenol molecules.

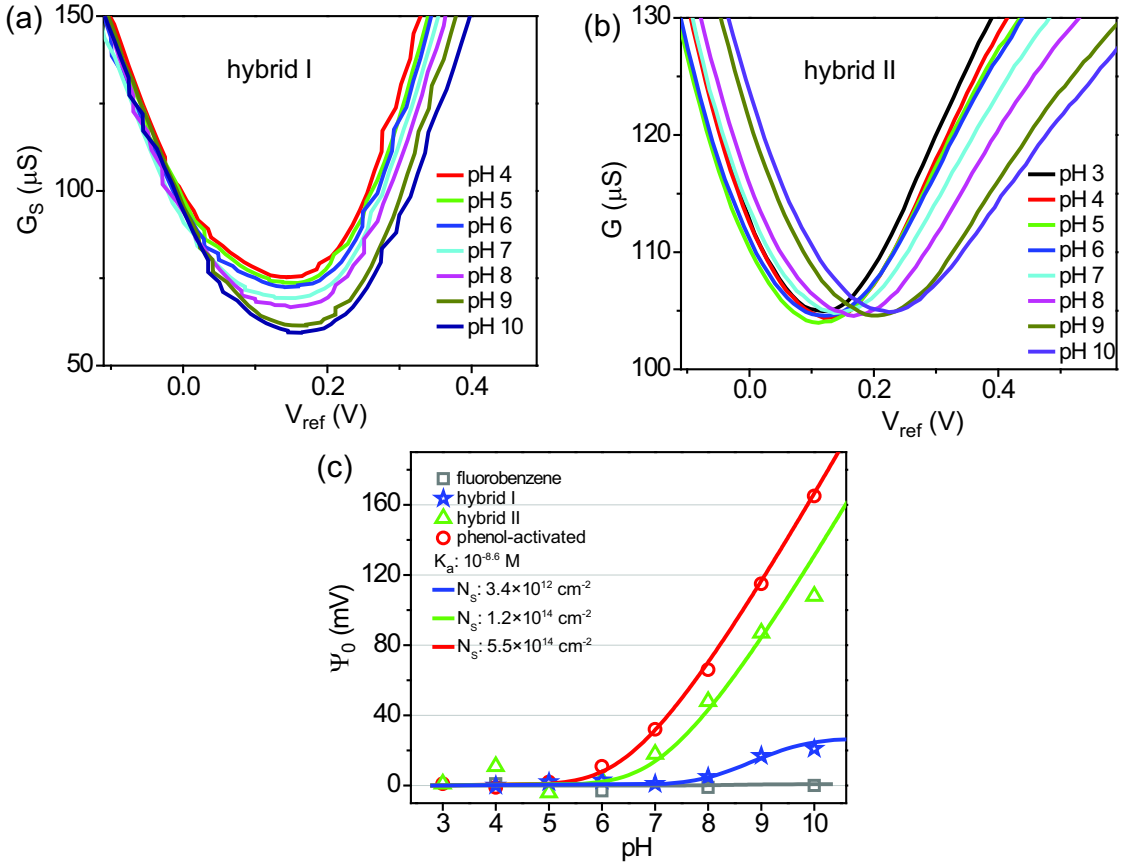

Figure S2: Electrical sheet conductance G_S and two-point electrical conductance G as a function of the reference potential V_{ref} measured in different pH buffer solutions for the hybrid I (a) and the hybrid II (b) phenol-fluorobenzene GISFETs, respectively. (c) Change of the surface potential Ψ_0 of the GISFETs vs. pH. Solid curves are fits to the single-reaction model with an equilibrium constant of $10^{-8.6}$ M. Note, the data points for fluorobenzene (grey squares) and phenol (red circles) have been shown in the manuscript as well.

Calculation of carrier mobility

In order to calculate the carrier mobility using $\mu = \frac{\delta G}{e\delta n}$, we first need to convert the gate voltage V_{ref} to carrier density n. As we known, the interfacial capacitance of a liquid-gated graphene FET can be modeled as two capacitors in series. One is the quantum capacitance of graphene, C_Q, that can be expressed in terms of carrier density: $C_Q = \frac{e^2\sqrt{n}}{h v_F \sqrt{\pi}}$ (Xia et al., *Nat. Nanotech.* 4, 505, **2009**), where h is the reduced Planck's constant, v_F is the Fermi velocity of the Dirac electron in graphene. The other is the double layer capacitance, C_{DL}, which is independent to the gate voltage. The potential dropped on the interface is then given by:

$$\left|V_{ref} - V_{CNP}\right| = \frac{h v_F \sqrt{\pi n}}{e} + \frac{en}{C_{DL}} \qquad (S1)$$

In Fig. S3a and b, we show the measured $G(V_{ref})$ curve of a graphene FET device in 100 mM KCl solution and the corresponding $G(n)$ obtained by using Eq. S1, respectively. Note, in case of high ionic strength, $C_{DL} \approx 20\,\mu$F/cm^2 is orders of magnitude larger than C_Q near CNP at low carrier density. We can easily calculate the carrier mobility of graphene from the slope of linear regimes of the $G(n)$ in Fig. S3b using $\mu = \frac{\delta G}{e\delta n}$. The obtained carrier mobilities are 800 cm^{2}V^{-1}s^{-1} for hole and 1100 cm^{2}V^{-1}s^{-1} for electron. As a comparison, we have performed Hall measurement of the device at the same time. The result is depicted in Fig. S3c, and we can calculate a hole and a electron Hall mobilities of 650 cm^{2}V^{-1}s^{-1} and 1700 cm^{2}V^{-1}s^{-1}, respectively (Fig. S3d). It is clear that the simple method using relation $\mu = \frac{\delta G}{e\delta n}$ gives a good estimation of the mobility. The calculated carrier mobilities as well as the minimum conductances of up to six as-fabricated and functionalized graphene FETs, are summarized in Tab. 1 in the main text. It is clear that the functionalization of graphene with aromatic molecules preserves its high mobility and conductance. Two third of the graphene FET devices exhibit a noticeable increase in the mobility after aromatic functionalization. Further investigations are required to identify the underlying mechanism.

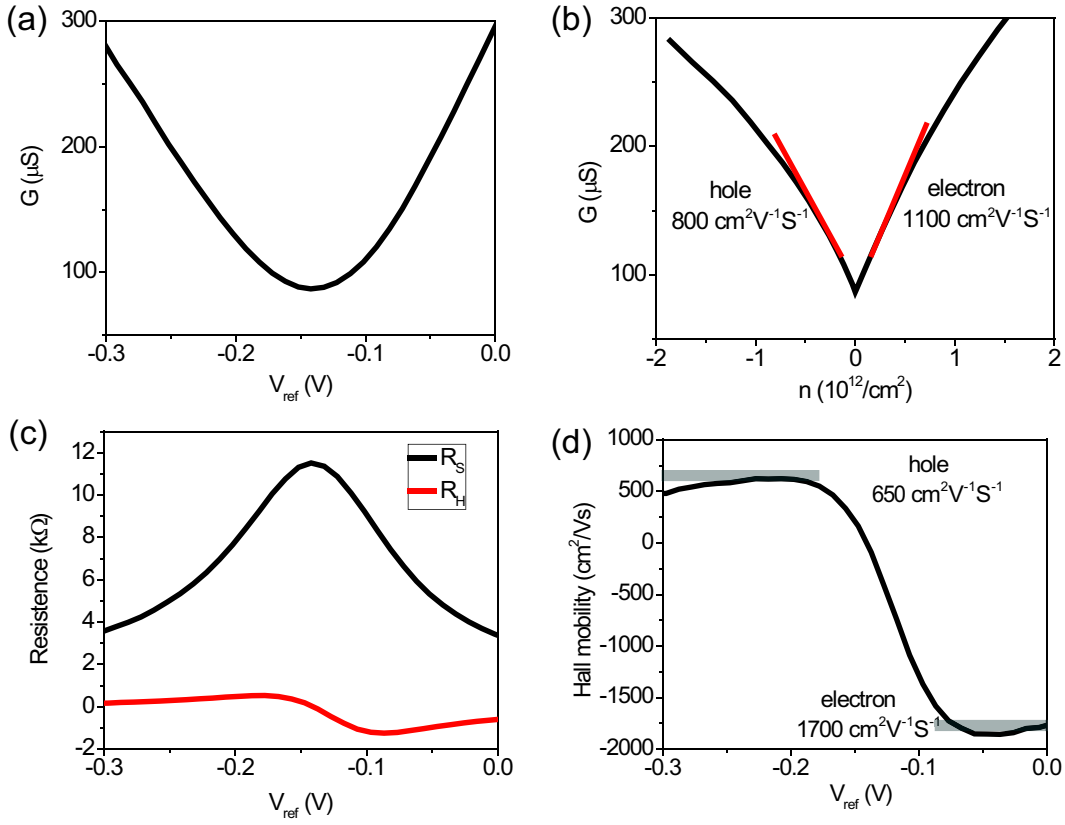

Figure S3: Mobility calculation. (a) and (b) The measured $G(V_{ref})$ curve of a graphene FET device in 100 mM KCl solution and its corresponding $G(n)$ curve, respectively. (c) The sheet and Hall resistance, R_S and R_H, as a function of reference gate voltage V_{ref} ranging from -0.3 V to 0 V. The measurement was performed at room temperatures with a magnetic field of $B = 0.4$ T in a home-made electromagnet. (d) The mobility away from CNP can be deduced by using the relation: $\mu = \frac{R_H}{R_S}$.

Low frequency noise spectrum of the phenol-activated GISFET

The noise power spectral density of the voltage fluctuations S_V (for more details, please refer to Tarasov and Fu et al., *Appl. Phys. Lett.* 90, 012114, **2011**) of the phenol-activated GISFET, was measured in pH 7 buffer solution at V_{ref} of -61 mV (at CNP) and 37 mV and depicted in Fig. S4a. The overlapping of the two S_V curves is consistent with the observations of previous literature (Cheng et al., *Nano Lett.* 10, 1864, **2010**). Here, the corresponding thermal background noise, recorded at zero bias, has been subtracted from the data. The S_V has a $1/f$ dependence (dashed lines), and its amplitude is proportional to V_{SD}^2 (not shown here). Such a behavior can phenomenologically be described by Hooge's law: $S_V = \frac{V_{SD}^2 \alpha}{Nf}$, where α is a material dependent constant and N denotes the number of fluctuators in the system.

We focus on determining the resolution limit and expressing it in a noise equivalent CNP voltage shift $\delta V_{CNP} = \frac{\sqrt{S_V/V_{SD}^2(f)}}{(lnG_S)'}$. In Fig. S4b, we reproduce the $G_S(V_{ref})$ of the phenol-activated GISFET at pH 7 and its corresponding derivative in natural logarithm $[(lnG_S)' = \frac{g}{G_S}]$, where $g = \frac{\delta G_S}{\delta V_{ref}}$ denotes the transconductance. In the optimized case (for example, V_{ref} =37 mV as indicated by dashed line in Fig. S4b), $\delta V_{CNP} = 1.8 \times 10^{-7}$ V/Hz$^{\frac{1}{2}}$ at 10 Hz frequency. Considering a pH response of 49 mV/pH for this device, we can determine a resolution limit of 4 ppm for a pH change in 1 Hz bandwidth, which is far superior to that of the-state-of-art commercial pH meters (0.1 %).

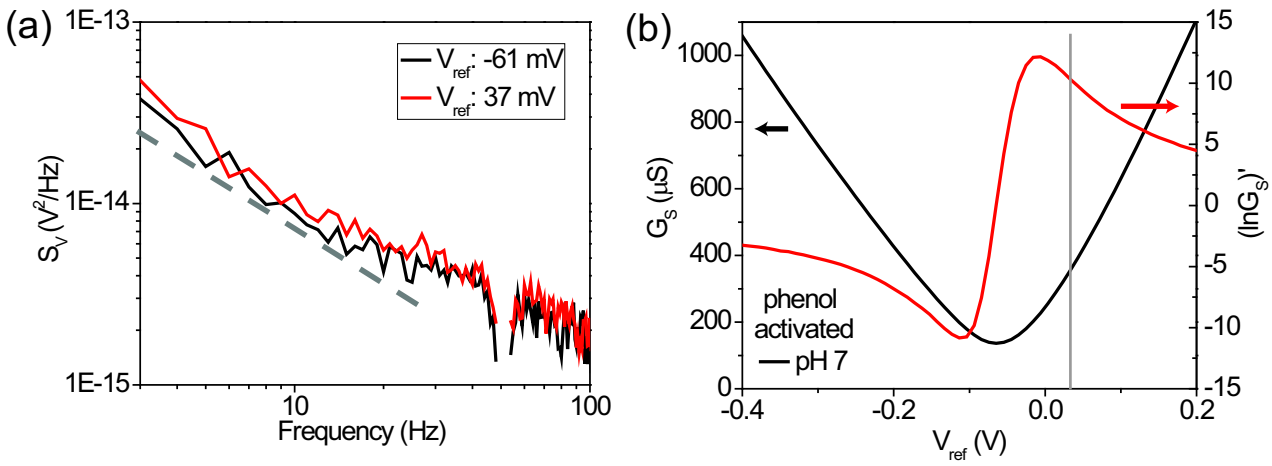

Figure S4: (a) The noise power spectral density of the voltage fluctuations S_V obtained for a source-drain bias voltage of $V_{SD} = 50\,\mathrm{mV}$ of the phenol-activated GISFET measured in pH 7 buffer solution. The dashed lines indicate a 1/f slope. (b) The $G_S(V_{ref})$ of the phenol-activated GISFET at pH 7 and its corresponding $(\ln G_S)'$. The grey line indicates V_{ref} =37 mV.

Single-reaction model

The OH surface group of a phenol molecular can be expressed by the equilibrium constant for the deprotonation (K_a):

$$C_6H_5OH \rightleftharpoons C_6H_5O^- + H_s^+, K_a = \frac{\nu_{C_6H_5O^-} \cdot a_{H_s^+}}{\nu_{C_6H_5OH}} \quad (S2)$$

with ν being the number of sites of one particular species, $a_{H_s^+}$ the activity of the surface protons. The active surface sites are either neutral (C_6H_5OH), or negatively charged (deprotonated, $C_6H_5O^-$). The total number of these sites is:

$$N_s = \nu_{C_6H_5OH} + \nu_{C_6H_5O^-} \quad (S3)$$

The deprotonated groups generate the total surface charge:

$$\sigma_0 = \left(-\nu_{C_6H_5O^-}\right) e \quad (S4)$$

Eq. S2 can be rewritten using Eq. S3-4:

$$\sigma_0 = eN_s \left(\frac{-K_a}{a_{H_s^+} + K_a} \right) \quad (S5)$$

The surface charge σ_0 is screened by the ions of the double layer, leading to a surface potential drop Ψ_0 over the double-layer capacitance C_{DL}:

$$\sigma_0 = C_{DL} \cdot \Psi_0 \quad (S6)$$

In order to get a convenient expression, the (unknown) activity of the surface protons in Eq. S6 has to be replaced by the (known) activity of the bulk solution protons $a_{H_b^+}$ *via* the Boltzmann

equation:

$$a_{H_s^+} = a_{H_b^+} \cdot \exp\left(-\frac{e\Psi_0}{kT}\right) \tag{S7}$$

Combining Eq. S2-7, an explicit relationship between the bulk proton activity a_{H_b} and the surface potential Ψ_0 can be derived:

$$a_{H_b^+} = -K_a \cdot \exp\left(\frac{e\Psi_0}{kT}\right) \cdot \left(1 + \frac{eN_s}{C_{DL}\Psi_0}\right) \tag{S8}$$

In case of 18-crown-6-potassium cation system, the mechanism can be modeled the same way as we described above, yielding:

$$a_{KCl} = K_{a-ce} \cdot \exp\left(\frac{e\Psi_0}{kT}\right) \cdot \left(\frac{eN_s}{C_{DL}\Psi_0} - 1\right) \tag{S9}$$

where a_{KCl} is the activity of KCl, K_{a-ce} is the equilibrium constant of the crown ether.

It should be noted that C_{DL} is not a constant at low ionic concentrations, but this can be considered as a secondary effect because only a small amount of K^+ binds to crown ether in this case.